

UNIVERSIDADE ESTADUAL DE CAMPINAS
SISTEMA DE BIBLIOTECAS DA UNICAMP
REPOSITÓRIO DA PRODUÇÃO CIENTÍFICA E INTELLECTUAL DA UNICAMP

Versão do arquivo anexado / Version of attached file:

Versão do Editor / Published Version

Mais informações no site da editora / Further information on publisher's website:

<https://opg.optica.org/oe/fulltext.cfm?uri=oe-21-22-25985&id=269975>

DOI: 10.1364/OE.21.025985

Direitos autorais / Publisher's copyright statement:

©2013 by Optical Society of America. All rights reserved.

DIRETORIA DE TRATAMENTO DA INFORMAÇÃO

Cidade Universitária Zeferino Vaz Barão Geraldo

CEP 13083-970 – Campinas SP

Fone: (19) 3521-6493

<http://www.repositorio.unicamp.br>

Carrier saturation in multiple quantum well metallo-dielectric semiconductor nanolaser: Is bulk material a better choice for gain media?

Felipe Vallini,^{1,*} Qing Gu,² Michael Kats,² Yeshaiah Fainman,² and Newton C. Frateschi¹

¹Device Research Laboratory, Applied Physics Department, "Gleb Wataghin" Physics Institute, University of Campinas - UNICAMP, 13083-859 Campinas, SP, Brazil

²Department of Electrical and Computer Engineering, University of California at San Diego, La Jolla, CA 92093-0407 USA

*fvallini@ifi.unicamp.br

Abstract: Although multi quantum well (MQW) structure is frequently suggested as the appropriate medium for providing optical gain in nanolasers with low threshold current, we demonstrate that in general bulk gain medium can be a better choice. We show that the high threshold gain required for nanolasers demands high threshold carrier concentrations and therefore a highly degenerate condition in which the barriers between the quantum wells are heavily pumped. As a result, there occurs spontaneous emission from the barrier in very dissipative low Q modes or undesired confined higher Q modes with resonance wavelengths close to the barrier bandgap. This results in a competition between wells and barriers that suppresses lasing. A complete model involving the optical properties of the resonant cavity combined with the carrier injection in the multilayer structure is presented to support our argument. With this theoretical model we show that while lasing is achieved in the nanolaser with bulk gain media, the nanolaser with MQW gain structure exhibits well emission saturation due to the onset of barrier emission.

©2013 Optical Society of America

OCIS codes: (140.3948) Microcavity devices; (140.5960) Semiconductor lasers.

References and links

1. R. F. Oulton, V. J. Sorger, T. Zentgraf, R. M. Ma, C. Gladden, L. Dai, G. Bartal, and X. Zhang, "Plasmon lasers at deep subwavelength scale," *Nature* **461**(7264), 629–632 (2009).
2. M. A. Noginov, G. Zhu, A. M. Belgrave, R. Bakker, V. M. Shalae, E. E. Narimanov, S. Stout, E. Herz, T. Suteewong, and U. Wiesner, "Demonstration of a spaser-based nanolaser," *Nature* **460**(7259), 1110–1112 (2009).
3. M. Khajavikhan, A. Simic, M. Katz, J. H. Lee, B. Slutsky, A. Mizrahi, V. Lomakin, and Y. Fainman, "Thresholdless nanoscale coaxial lasers," *Nature* **482**(7384), 204–207 (2012).
4. S. Kita, S. Hachuda, S. Otsuka, T. Endo, Y. Imai, Y. Nishijima, H. Misawa, and T. Baba, "Super-sensitivity in label-free protein sensing using a nanoslot nanolaser," *Opt. Express* **19**(18), 17683–17690 (2011).
5. G. Roelkens, L. Liu, D. Liang, R. Jones, A. W. Fang, B. Koch, and J. E. Bowers, "III-V/silicon photonics for on-chip and intra-chip optical interconnects," *Laser Photon. Rev.* **4**(6), 751–779 (2010).
6. S. Noda, "Applied physics. Seeking the ultimate nanolaser," *Science* **314**(5797), 260–261 (2006).
7. O. Painter, R. K. Lee, A. Scherer, A. Yariv, J. D. O'Brien, P. D. Dapkus, and I. Kim, "Two-dimensional photonic band-gap defect mode laser," *Science* **284**(5421), 1819–1821 (1999).
8. B. Ellis, M. A. Mayer, G. Shambat, T. Sarmiento, J. Harris, E. E. Haller, and J. Vučković, "Ultralow-threshold electrically pumped quantum-dot photonic-crystal nanocavity laser," *Nat. Photonics* **5**(5), 297–300 (2011).
9. M. H. Huang, S. Mao, H. Feick, H. Q. Yan, Y. Y. Wu, H. Kind, E. Weber, R. Russo, and P. D. Yang, "Room-temperature ultraviolet nanowire nanolasers," *Science* **292**(5523), 1897–1899 (2001).
10. A. H. Chin, S. Vaddiraju, A. V. Maslov, C. Z. Ning, M. K. Sunkara, and M. Meyyappan, "Near-infrared semiconductor subwavelength-wire lasers," *Appl. Phys. Lett.* **88**(16), 163115 (2006).
11. C. Z. Ning, "Semiconductor nanolasers," *Phys. Status Solidi B* **247**, 774–788 (2010).

12. M. T. Hill, Y. S. Oei, B. Smalbrugge, Y. Zhu, T. de Vries, P. J. van Veldhoven, F. W. M. van Otten, T. J. Eijkemans, J. P. Turkiewicz, H. de Waardt, E. J. Geluk, S. H. Kwon, Y. H. Lee, R. Nötzel, and M. K. Smit, "Lasing in metallic-coated nanocavities," *Nat. Photonics* **1**(10), 589–594 (2007).
13. M. T. Hill, M. Marell, E. S. P. Leong, B. Smalbrugge, Y. Zhu, M. Sun, P. J. van Veldhoven, E. J. Geluk, F. Karouta, Y. S. Oei, R. Nötzel, C. Z. Ning, and M. K. Smit, "Lasing in metal-insulator-metal sub-wavelength plasmonic waveguides," *Opt. Express* **17**(13), 11107–11112 (2009).
14. K. Yu, A. Lakhani, and M. C. Wu, "Subwavelength metal-optic semiconductor nanopatch lasers," *Opt. Express* **18**(9), 8790–8799 (2010).
15. S. H. Kwon, J. H. Kang, C. Seassal, S. K. Kim, P. Regreny, Y. H. Lee, C. M. Lieber, and H. G. Park, "Subwavelength plasmonic lasing from a semiconductor nanodisk with silver nanopan cavity," *Nano Lett.* **10**(9), 3679–3683 (2010).
16. M. P. Nezhad, A. Simic, O. Bondarenko, B. Slutsky, A. Mizrahi, L. Feng, V. Lomakin, and Y. Fainman, "Room-temperature subwavelength metallo-dielectric lasers," *Nat. Photonics* **4**(6), 395–399 (2010).
17. A. Mizrahi, V. Lomakin, B. A. Slutsky, M. P. Nezhad, L. Feng, and Y. Fainman, "Low threshold gain metal coated laser nanoresonators," *Opt. Lett.* **33**(11), 1261–1263 (2008).
18. Q. Ding, A. Mizrahi, Y. Fainman, and V. Lomakin, "Dielectric shielded nanoscale patch laser resonators," *Opt. Lett.* **36**(10), 1812–1814 (2011).
19. A. Matsudaira, C. Y. Lu, M. Zhang, S. L. Chuang, E. Stock, and D. Bimberg, "Cavity-volume scaling law of quantum-dot metal-cavity surface-emitting microlasers," *IEEE Photon. J.* **4**(4), 1103–1114 (2012).
20. K. Ding, M. T. Hill, Z. C. Liu, L. J. Yin, P. J. van Veldhoven, and C. Z. Ning, "Record performance of electrical injection sub-wavelength metallic-cavity semiconductor lasers at room temperature," *Opt. Express* **21**(4), 4728–4733 (2013).
21. D. Bajoni, "Polariton lasers. Hybrid light-matter lasers without inversion," *J. Phys. D* **45**(31), 313001 (2012).
22. P. Bhattacharya, B. Xiao, A. Das, S. Bhowmick, and J. Heo, "Solid state electrically injected exciton-polariton laser," *Phys. Rev. Lett.* **110**(20), 206403 (2013).
23. W. Rideout, W. F. Sharfin, E. S. Koteles, M. O. Vassell, and B. Elman, "Well-barrier hole burning in quantum well lasers," *IEEE Photon. Technol. Lett.* **3**(9), 784–786 (1991).
24. T. Kouno, K. Kishino, T. Suzuki, and M. Sakai, "Lasing actions in GaN tiny hexagonal nanoring resonators," *IEEE Photon. J.* **2**(6), 1027–1033 (2010).
25. F. Vallini, Q. Gu, B. Wingad, B. Slutsky, M. Katz, Y. Fainman, and N. C. Frateschi, "Geometry optimization of nanopatch semiconductor lasers: the trade-off between quality factor and gain," in *Latin America Optics and Photonics Conference, Technical Digest* (online) (Optical Society of America, 2012), paper LT3B.2.
26. M. Rosenzweig, M. Möhrle, H. Düser, and H. Venghaus, "Threshold current analysis of InGaAs-InGaAsP multiquantum well separate-confinement lasers," *IEEE J. Quantum Electron.* **27**(6), 1804–1811 (1991).
27. S. L. Chuang, *Physics of Optoelectronic Devices* (New York, Wiley, 1995), Chap. 9.
28. A. R. Reisinger, P. S. Zory, and R. G. Waters, "Cavity length dependence of the threshold behavior in thin quantum well semiconductor lasers," *IEEE J. Quantum Electron.* **23**(6), 993–999 (1987).
29. C. M. Wu and E. S. Yang, "Physical mechanisms of carrier leakage in DH injection lasers," *J. Appl. Phys.* **49**(31), 14–31 (1978).
30. H. C. Casey, Jr., "Room-temperature threshold current dependence of GaAs-AlxGa1-xAs double heterostructure lasers on x and active layer thickness," *J. Appl. Phys.* **49**(7), 3684–3692 (1978).
31. N. K. Dutta, "Calculated temperature dependence of threshold current of GaAs-AlxGa1-xAs double heterostructure lasers," *J. Appl. Phys.* **52**(1), 70–73 (1981).
32. K. Y. Lau, "Dynamics of quantum well lasers," in *Quantum Well Lasers*, P. S. Zory ed., Quantum Well Lasers, (Academic, San Diego, Cal., 1993).
33. R. Nagarajan, M. Ishikawa, T. Fukushima, R. S. Geels, and J. E. Bowers, "High speed quantum-well lasers and carrier transport effects," *IEEE J. Quantum Electron.* **28**(10), 1990–2008 (1992).
34. L. A. Coldren, S. W. Corzine, and M. L. Mashanovitch, *Diode Lasers and Photonic Integrated Circuits*. (New York, Wiley, 2012), Chap. 5.
35. M. Fujita, A. Sakai, and T. Baba, "Ultrasmall and ultralow threshold GaInAsP-InP microdisk injection lasers: design, fabrication, lasing characteristics, and spontaneous emission factor," *IEEE J. Sel. Top. Quantum Electron.* **5**(3), 673–681 (1999).

1. Introduction

The demonstration of room temperature electrically pumped semiconductor nanolasers has been of great interest in recent years. This interest has two main motivations: (a) fundamental physics involving matter and radiation interaction in small volumes, and (b) technology for the high density integration of coherent light sources in photonic circuits.

An interesting avenue of fundamental physics enabled by the reduction of the laser size to dimensions comparable to the emission wavelength is the ability to tailor the spontaneous emission and, consequently, of the stimulated emission. This ability has enabled the

demonstration of new classes of nanolasers such as plasmonic nanolasers and thresholdless semiconductor nanolasers employing optical pumping [1–3].

The ability to produce small, high-density, high-efficiency nanolasers will have wide-ranging technological applications. Nanolasers will be useful for ultrahigh resolution and high-throughput imaging, sensing and spectroscopy systems, all with low power consumption and with the coherent light source integrated with the sensor, reducing the fabrication cost of such devices [4]. In optical telecommunications, semiconductor nanolasers can produce on-chip high density optical interconnects with very low power consumption [5]. These nanolasers will need to be electrically pumped, and will need to have small footprints [6]. To achieve this, two major issues have to be considered: the architecture for photonic confinement and the choice of material for the optical gain region. Finally, a design for efficient electrical pumping is essential.

The first important aspect of design is to choose the method of photonic confinement for the optical cavity. Several efforts have been directed towards reaching high performance room temperature electrically pumped semiconductor nanolasers, using several different strategies toward achieving optical confinement. The lowest threshold current laser was obtained with quantum dots as the active material inserted in a high quality factor (Q) resonant cavity in 2D photonic crystal structures [7,8]. However, although the photonic concentration in these devices is high, the footprint is very large. One approach to drastically reduce the footprint is to use semiconductor nanowires [9,10]. However, current injection is very difficult in these devices [11]. An alternative approach is the metallic-coated resonator design [12–15]. These resonators may be designed to employ plasmonic confinement that allows hybridization of plasmonic and dielectric modes [13]. The intrinsic insertion loss within the conductor is the major challenge with this approach. The third approach is to use a design that minimizes the conductor optical losses by reducing the optical mode overlap with the metal and, at the same time, reduces the radiation losses, also known as the metallo-dielectric design [16–18]. This is the approach of choice in our work. In order to pursue this approach, inherent issues such as self-heating generated by current injection and the high series resistance caused by the inherent small injection area need to be addressed [19]. This demands the optimization of the ohmic contact as well as a search for a design, which, while providing high photonic confinement, does not impair the current injection, leading to small threshold currents.

The second important aspect of design is the electron confinement and material choice for the active region of the device. To our knowledge, metallo-dielectric resonators have employed bulk alloy $\text{In}_{0.53}\text{Ga}_{0.47}\text{As}$ material as the active medium inside a double heterostructure for current injection and electron confinement. These are the only demonstrated metallo-dielectric semiconductor electrically pumped nanolasers, operating from cryogenic to room temperatures. Unfortunately, the threshold current, the required material gain and self-heating effects are still high and need to be reduced for an efficient operating device. A frequent suggestion found in the literature is to employ quantum wells (QW's) as the gain media [20]. The interest on QW material relies on their lower transparent carrier density in comparison with bulk materials, which allows lower threshold currents due to the higher material gain and power consumption. More than that, quantum well engineering allows the tailoring of the emission wavelength which is used to adjust the laser wavelength to the several available wavelength division multiplexing (WDM) channels. Another possibility of using QW's is to generate coherent emission of light through the decay of exciton-polaritons, which is called an inversionless laser and have a very small threshold current compared to a photon laser [21]. Unfortunately such devices operate at cryogenic temperatures or with a large magnetic field applied to them due to the very small binding energy of the excitons [21,22].

Besides all the above-mentioned advantages of using QW as gain media, these structures present some disadvantages that can explain why metallo-dielectric semiconductor

electrically pumped nanolasers with QW active region have not been demonstrated yet. First, the confinement factor in MQW gain media is very low in comparison with a bulk gain media, which makes the modal threshold gain to be lower for the bulk. Second, not yet widely discussed in the nanolaser literature, is the leakage of carriers to the barriers. As the photonic radiation losses become very high and the gain medium size diminishes, such as in the case of nanolasers, very high injected carrier density is necessary to achieve a material gain to overcome such radiation losses. This regime of high excitation leads to a large separation between the electron and hole quasi-Fermi levels. This, in turn, leads to barrier pumping as well as the saturation of the carrier concentration and of the material gain within the QW [23]. Finally, one could argue that barrier population can be prevented or minimized by increasing the barrier height without changing the well height. However, in order to achieve the threshold material gain, structures with several quantum wells (MQW) are necessary. The taller the barriers, the more inhomogeneous the population in the wells becomes. Inhomogeneous pumping is extremely detrimental for achieving the threshold condition.

In this work, we show that this effect indeed limits the use of QW as the active medium in nanolasers. In other words, we will show that although QW are very suitable for reducing the threshold current in large lasers, bulk material is better for these nanostructures. In order to quantitatively analyze this effect, we designed metallo-dielectric cavities with (a) MQW and (b) bulk active media. Our interest lies in the optical telecommunication wavelengths, particularly the C band region (1530 nm to 1565 nm), so the gain material used is based on InGaAsP (III-V) alloys. We optimized both cavity designs and used rate equations accounting for diffusion of carriers within the barriers for the MQW structure. We show that the MQW device tends to have its gain saturated with the onset of emission from the barriers. As a result, lasing in the fundamental mode is only achieved with the bulk gain device.

2. Semiconductor nanolasers current injection

In order to qualitatively understand the dependence of the carrier population on current injection for the bulk and for the MQW active region, we have simulated the band diagram of both structures when unbiased, under small bias and large bias. In all cases, the gain medium is placed within a double heterostructure P-i-N diode. The structure is as follows: semi-insulating InP substrate, 1 μm $\text{p}^+\text{-In}_{0.733}\text{Ga}_{0.227}\text{As}_{0.493}\text{P}_{0.507}$ layer, 1 μm p-InP layer, 10 quantum wells consisting of 100 \AA $\text{In}_{0.56}\text{Ga}_{0.44}\text{As}_{0.938}\text{P}_{0.062}$ ($E_g = 0.761$ eV) wells within 200 \AA $\text{In}_{0.734}\text{Ga}_{0.266}\text{As}_{0.571}\text{P}_{0.429}$ ($E_g = 0.954$ eV) barriers, 0.2 μm n-InP layer and a 0.125 μm $\text{n}^+\text{-In}_{0.53}\text{Ga}_{0.47}\text{As}$ layer. The highly doped layers are used for the ohmic contact formation, the doped InP layers are the cladding layers, and the MQW layers form the active region. In the case of bulk active region, we considered an $\text{In}_{0.53}\text{Ga}_{0.47}\text{As}$ layer replacing the MQW. All layers are lattice matched to InP and the active region thickness is 400 nm for both cases. The band diagram simulations were performed using the software SILVACO which solves self-consistently the Poisson equation, the Schrodinger equation and the carrier transport equations. Figures 1(a) and 1(c) show the unbiased band diagrams for the MQW and the bulk gain structures, respectively. Considering only the semiconductor layers, we define the material width in the simulation such that the gain medium volume is $\sim 0.23\mu\text{m}^3$, which is on the same order of typical nanolaser cavities [20]. E_{fc} and E_{fv} are the quasi-Fermi levels for the electrons and for the holes, respectively. Figures 1(b) and 1(d) show the biased band diagrams for the MQW and the bulk gain structures, respectively. Two biases conditions are displayed: the dashed red line is obtained under a low bias (around 0.8 V) and the blue dashed line is obtained under a higher bias condition (around 1.0 V). For the bulk gain structure we observe the band filling effect since the E_{fc} and E_{fv} separation shifts the band edges towards shorter wavelengths. On the other hand, for the MQW gain structures, the barriers become populated in the high injection regime. As a result, the increase of the well carrier density with bias becomes smaller and eventually stops. Under optical pumping condition, the same problem exists since carrier density within the QW is univocally dependent upon the quasi-Fermi level

separation. However, without the self heating effects of current injection, lower gain threshold requirement may permit lasing at the well wavelength. In fact, optically pumped MQW nanolasers have already been demonstrated [3,15].

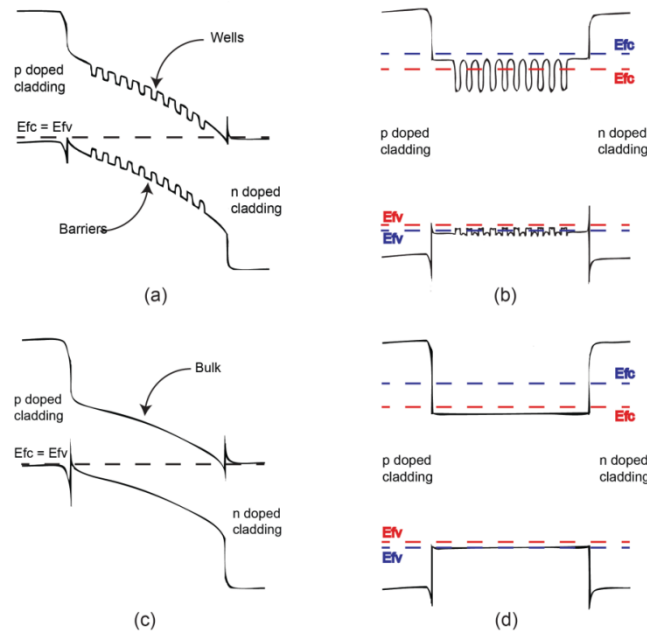


Fig. 1. Simulated band diagrams with the electrons and holes quasi-Fermi levels (E_{fc} and E_{fv}) of a (a) unbiased MQW heterostructure; (b) forward biased MQW heterostructure; (c) unbiased bulk heterostructure and (d) forward biased bulk heterostructure. Red dashed lines are for 0.8 V bias and blue dashed lines are for 1.0 V bias.

3. Optical cavity and material gain optimization

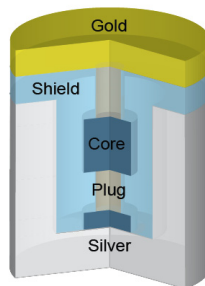


Fig. 2. Schematics of a nanopatch laser resonator.

Fabry-Perot nano cavity lasers, disk resonators, ring resonators and nanopatch resonators have been experimentally demonstrated and/or proposed for metallo-dielectric electrically pumped semiconductor nanolasers [12,14,15,24]. Since our analysis of comparing MQW and bulk gain media should not depend upon a particular cavity design, we have chosen to explore the nanopatch semiconductor laser, a metallo-dielectric resonator proposed by Q. Ding et. al. because it is a strong candidate for planar integration with silicon based photonics and due to its high spontaneous emission into laser mode (β -factor) [18]. A schematic drawing of the device is shown in Fig. 2. The MQW (bulk) gain device consists of a 190 (185) nm radius cylindrical gain core held by two 150 (185) nm radius InP cylindrical plugs. One should notice that the core and plug have the same radius for the optimized bulk gain resonator, i.e.,

there is no undercut in this case. The optimization is based on the optical confinement and carrier injection as discussed in the next sub-sections. A 200 nm thick silicon dioxide conformal layer is deposited on the plugs and core. The entire structure is surrounded by 300 nm of silver and covered by a 300 nm layer of gold as shown in Fig. 2. The silicon dioxide shield layer is designed to reduce the overlap between the optical mode and the metal [17]. The silver and gold thicknesses are designed such that they can act as an antenna to couple light to an adjacent waveguide [18]. The total height of the structure is 1550 nm.

The optimization of core and plug radii for each case was performed as follows [25]: we varied both radii from 100 nm to 200 nm minimizing the calculated threshold current. The minimum radius is limited by the resolution of fabrication, while the maximum radius is limited by the onset of degenerate multimode behavior in the 1550 nm emission range.

3.1. Modal calculation

Finite element simulation with the software COMSOL was used for the modal calculation. As the core and the plug radii change, the resonant mode wavelength, the confinement factor Γ and quality factor Q change. The inset of Fig. 3(a) titled QW and the inset of Fig. 3(b) titled Bulk #1 contains the spatial distribution and the modal properties for the first order confined optical mode. For both cases the resonant mode is the axial symmetric TE_{011} .

3.2. Calculation of threshold current

Assuming metallic and radiation losses, we can then obtain the lasing threshold gain g_{th} as a function of the mode wavelength, as shown by the green curves in Figs. 3(a) and 3(b) for MQW and bulk gain, respectively. Since the resonant wavelength range is different for each structure, the range of calculation was increased to facilitate the comparison between the two structures. For each core and plug radius in our range, we calculate the material gain for the resulting structure (as described in the following sub-section), and then use our calculated gain versus carrier concentration relation to calculate threshold carrier density to reach g_{th} for each structure. Considering the emission within the range of 1500 to 1610 nm one searches for the minimum threshold current. To calculate the threshold current necessary to populate the active gain medium with the threshold carrier density, we use the software SILVACO, which self-consistently solves the Poisson equation, the Schrodinger equation, and the carrier transport equations considering Fermi Dirac statistics. The threshold current sets the desired optimum core and plug radii with the respective resonance wavelengths shown by vertical dashed red lines in Fig. 3(a), at 1562.7 nm, and Fig. 3(b), at 1602.1 nm.

3.3. Calculation of material gain

The material gain for both gain media was calculated based on the reduced effective mass approach, Fermi Dirac statistics and intraband scattering broadening. In the case of the MQW medium, we include both the bound (energy lower than the barrier height) and unbound (energy higher than the barrier height) electrons [26,27]. Due to the shallow height of the barrier, there is only one quantized energy level for the electrons in the conduction band and three quantized levels for the holes in the valence band: two for the heavy hole bands and one for the light hole band. Since the transition from the conduction band level to the second heavy hole level is not allowed, and the density of states for the light hole is small, only the transition from the conduction band level to the first heavy hole level was considered in the calculations. Also, the barrier material optical gain was calculated considering the region as a bulk.

4. Results of cavity optimization and simulation: the role of barrier pumping

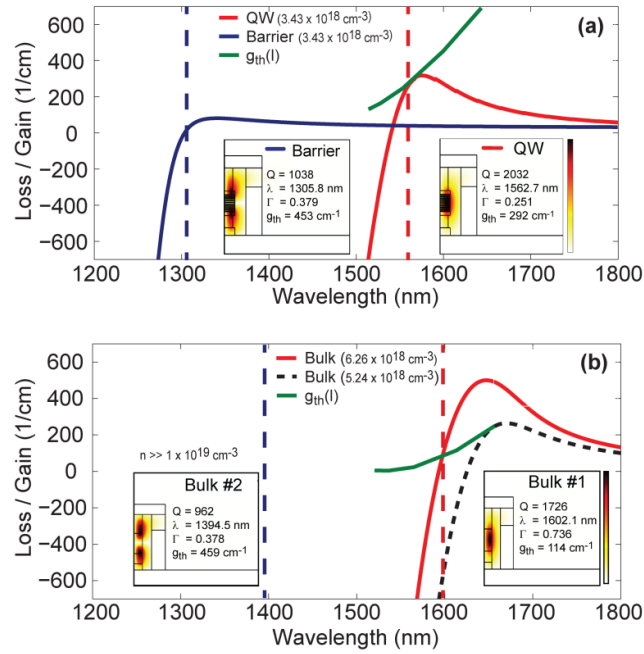


Fig. 3. Material gain dependence with wavelength for (a) an InGaAsP MQW structure (red) and an InGaAsP barrier (blue) at the threshold carrier density for the first order mode and (b) an InGaAsP bulk material for two different carrier densities, one at the threshold (red) and other for an optimized cavity (black dashed line). The green curves are the threshold gain dependence with resonance wavelength. Insets: possible confined optical modes and their properties. The thermal color scale indicates the normalized power from 0 (white) to 1 (black). The rightmost inset of Fig. 3(a) shows the fundamental mode (well mode) with a quality factor (Q) of 2032, resonance wavelength of 1562.7 nm, a confinement factor (Γ) of 0.251 and a threshold gain (g_{th}) of 292 cm⁻¹. The leftmost inset of Fig. 3(a) shows the second longitudinal mode (along the height direction), (barrier mode), with a Q of 1038, resonance wavelength of 1305.8 nm, a Γ of 0.379 and a g_{th} of 453 cm⁻¹. The insets of Fig. 3(b) also contain the first order mode and second longitudinal order mode for the bulk core media. The first mode, labeled Bulk #1, has a Q of 1726, resonance wavelength of 1602.1 nm, a Γ of 0.736 and a g_{th} of 114 cm⁻¹. The second order mode, labeled Bulk #2, has a Q of 962, resonance wavelength of 1394.5 nm, a Γ of 0.378 and a g_{th} of 459 cm⁻¹.

The red curves in Fig. 3 are the calculated material gain at the threshold carrier density for the first order mode. We observe that in Fig. 3(a), for the MQW, the maximum gain matches the threshold gain at the resonance wavelength. This is possible since one can optimize the well/barrier composition; a definite advantage of using MQW design. For the bulk case in Fig. 3(b) we notice that the same optimization is impossible unless the dimensions are changed beyond the established radii limits, causing a shift in resonance wavelengths, as shown by the black dashed line on Fig. 3(b), or one must use a quaternary (InGaAsP) alloy. In our study, we will keep the ternary alloy for the bulk gain media, even though it is not optimized. Therefore, in terms of gain/resonance overlap, the MQW material is more optimized for the nanopatch laser. A final important remark about the cavity design is the fact that it is very difficult to avoid the presence of high order modes with resonances near 1300 nm. The high order mode (second longitudinal mode), here called the barrier mode, shown in the inset of Fig. 3(a), with a Q of 1038, has resonance wavelength of 1305.8 nm, a Γ of 0.379 and a g_{th} of 453 cm⁻¹ for the MQW gain core. The second order mode for the bulk gain core, Bulk #2 on the inset of Fig. 3(b), has a Q of 962, resonance wavelength of 1394.5 nm, a Γ of 0.378 and a g_{th} of 459 cm⁻¹. The difference between the two cases is that material gain may be

available for the barrier mode for the MQW core when the quasi-Fermi level difference allows barrier population. The blue curve in Fig. 3(a) shows the calculated material gain of the barrier, considering the media as a bulk, at the threshold carrier density of the well mode. In fact, this second order mode is undesired but inherent to the cavity design. Since any modification to the design to prevent this mode would affect the fundamental mode which is already fully optimized, no optimization was performed to minimize the effect of the second order mode. Therefore, with the high carrier density needed for lasing at the 1560 nm resonance, a competition with this second order mode may cause yet more saturation for the well emission. This does not mean that the second order mode will reach its threshold; it means that the injected carriers will start populating the barrier together with the well levels. Since the density of states in the barrier (considered here as a bulk material) is higher than that in the well levels, the tendency is a saturation of carrier density in the wells. Even if there was no gain in the barrier the same saturation effect would be present since the barriers still consume carriers. Notice in Fig. 3(b) that no material gain is available in the bulk gain core near the second order resonance, at least at the moderately high carrier density shown. Also, the rightmost inset in Fig. 3(b) shows that the bulk design has a higher Γ compared with the MQW design.

In the following section, using the laser rate equations, we will compare the performance of the MQW gain structure, which has the advantage of being fully optimized, with the bulk gain structure, which has the advantage of having a higher confinement factor.

5. Semiconductor laser rate equation analysis

Reisinger *et al.* [28] comment that while quantum well lasers have very small threshold currents and are almost insensitive to the cavity length for long lasers, quantum wells are not suitable for very short lasers. In short nanolasers, leakage of carriers and other two non-radiative processes inherent to the materials: Auger recombination and recombination from L valleys are prominent, which are detrimental to device performance [28]. The effects of carrier leakage was introduced to the threshold current analysis to explain the sharp rise of the threshold current in very short quantum well lasers [29–31]. In this context, the carriers have enough energy to reach the barriers layers and be swept away by drift or diffusion, while carriers also decay by spontaneous emission or stimulated emission, if the cavity losses allow. Furthermore, the threshold gain for such small lasers leads to a dramatic increase in threshold current, and consequently, a collapse of the quantum efficiency. Lastly, if the wells allow, while the current increase, it is possible to have other transitions between the higher quantized levels, which means an emission wavelength shift. As already known, such wavelength shift can be detrimental for nanolasers, which have a very specific cavity design with a very sensitive resonant wavelength.

In our model, we include the carrier leakage to the barriers. The effects of barrier pumping on lasing were analyzed employing the reservoir model proposed by Rideout *et al.* [23]. In this model, we consider two reservoirs for carriers: one for the confined electrons (in the well) and the other for the unconfined electrons (in the barrier). These two reservoirs can exchange carriers with time constants τ_{cap} and τ_{esc} , for capture and escape respectively. The capture time describes electrons' displacement from the barrier to the well while the escape time is related to the opposite situation. These characteristic times are described by phonon-assisted quantum transitions, tunneling (which depends on effective barrier height and width as well as on the applied electric field), thermionic emission (which depends strongly on the effective barrier height), and classical carrier diffusion in each region [23,32]. Although the capture and escape dynamics depend on the effective barrier height, which in turn depends upon the quasi-Fermi levels, we will use average constant capture and escape times, as employed by other authors [32–34]. The full description of the dynamics would be needed to describe the modulation response of the device; however, this is beyond the scope of this work.

In order to apply this model, we construct a photonic rate equation at the well wavelength, a photonic rate equation at the barrier wavelength, a carrier rate equation for the well and a carrier rate equation for the barrier. For the MQW structure, we lumped all barrier regions together. Assuming uniform carrier distribution in the wells as did in the barriers, it is also possible to lump the well regions since the calculated gain is for the entire set of 10 wells. The rate equations are

$$\frac{dn_{\text{barrier}}}{dt} = \frac{I}{qV_{\text{barrier}}} - R_{\text{NR}} - R_{\text{barrier}} - \frac{n_{\text{barrier}}}{\tau_{\text{cap}}} + \frac{n_{\text{wells}}}{\tau_{\text{esc}}} \left(\frac{V_{\text{wells}}}{V_{\text{barrier}}} \right) - v_g p_{\text{barrier}} g_{\text{barrier}} \quad (1)$$

$$\frac{dn_{\text{wells}}}{dt} = \frac{n_{\text{barrier}}}{\tau_{\text{cap}}} \left(\frac{V_{\text{barrier}}}{V_{\text{wells}}} \right) - R_{\text{NR}} - R_{\text{wells}} - \frac{n_{\text{wells}}}{\tau_{\text{esc}}} - v_g p_{\text{wells}} g_{\text{wells}} \quad (2)$$

$$\frac{dp_{\text{barrier}}}{dt} = \Gamma_2 \beta_2 R_{\text{barrier}} + \left[\Gamma_2 v_g g_{\text{barrier}} - \frac{\omega_2}{Q_2} \right] p_{\text{barrier}} \quad (3)$$

$$\frac{dp_{\text{wells}}}{dt} = \Gamma_1 \beta_1 R_{\text{wells}} + \left[\Gamma_1 v_g g_{\text{wells}} - \frac{\omega_1}{Q_1} \right] p_{\text{wells}} \quad (4)$$

where n_{barrier} and n_{wells} are the lumped carrier densities in the barriers and in the wells respectively, I is the injection current, q is the electron charge, V_{barrier} and V_{wells} are the volume for the barrier and wells region respectively, R_{NR} is the non-radiative recombination rate, R_{barrier} is the spontaneous emission at the barrier, v_g is the group velocity, p_{barrier} and p_{wells} are the photon density at the barrier and at the wells respectively, g_{barrier} and g_{wells} are the material gain at the barrier and at the wells, R_{wells} is the spontaneous emission at the wells, β_1 and β_2 are the spontaneous emission coupling factors for first order and second order mode respectively, and ω_1 and ω_2 are the resonance frequency for the first order and second order mode respectively. The Purcell factor was not taken into account in our analyses. Its insertion in the model would affect almost equally the MQW and the bulk structures. It is well known each confined mode has different group velocities, but here we have considered them equal since the difference should not be meaningful in our analysis. The gain and all recombination rates are carrier density dependent. For non-radiative recombination rates, we have considered Auger effect and surface recombination. The surface recombination is the most relevant in the case of nanolasers since the area/volume ratio is very high due to their small features. Typical values for Auger coefficient and surface recombination velocity of $1.1 \times 10^{-31} \text{ cm}^6/\text{s}$ and $5 \times 10^4 \text{ cm/s}$ were considered, respectively. We calculate the dependence of material gain on carrier injection and wavelength using the same methods as described in the optimization procedure above. For τ_{cap} and τ_{esc} , typical theoretical values found in the literature were used: 60 and 300 ps respectively [32–34]. With such short characteristic times, thermal equilibrium of carriers can be assumed in the rate equation analysis.

The dynamic rate equations are solved until a steady state condition is reached. Figures 4(a) and 4(b) show the light output power calculated for the MQW and bulk gain respectively nanopatch lasers versus injected current ($L \times I$) for several β factors. To facilitate a clear comparison, the same β factors were used for both barrier and well modes. The solid lines are the $L \times I$ curves for the well mode and the dashed lines are for the barrier mode.

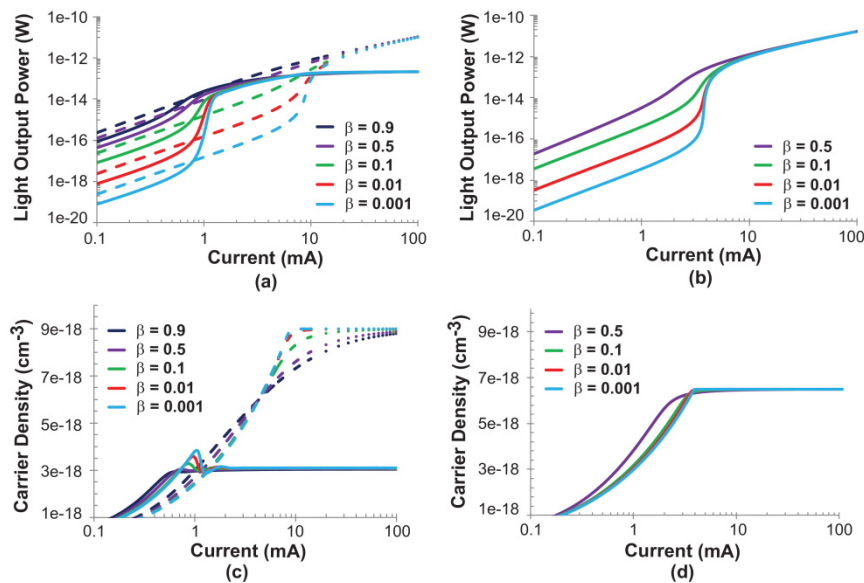


Fig. 4. Log-log curves of the light output power \times injection current for (a) MQW gain media and (b) bulk gain media with several β 's. (c) and (d) are the carrier density \times injection current for the MQW and bulk gain media respectively. The solid lines are for the first order mode while the dashed lines are for the second order mode. Note that in the MQW gain system, the second order mode is the barrier mode.

As depicted in Fig. 4(a), the emitted power from the barrier (dashed line) overcomes the well emission (solid line) when under low injected current. This happens because the radiation losses of total Q for the barrier mode is almost half the radiation losses of the total Q for the QW mode so the double of the light is expected from the barriers. Comparing the curves for the same mode the emitted power is proportional to the β -factor. Therefore, at these low currents, light output that is proportional to the radiation loss of the barrier mode is larger. With further increase in current, the well mode goes into the amplified spontaneous emission (ASE) regime, seen by the change of slope in the curves around 0.5 to 1 mA, while the barrier mode remains in the electro-luminescent regime. At this point, the well emission is higher than the barrier emission. If current is further increased, stimulated emission is dominant for the well mode, and all solid lines show that the system is close to the threshold condition. After this point, the curves suggest that the well mode has already passed threshold (which is commonly interpreted as the center point of the ASE regime at the inflexion point of the curve); however, the photon number doesn't rise linearly as it would in a single mode laser. Instead, the photon number stays constant due to the suppression of the well emission with the onset of barrier emission. If the well mode was the only resonant mode, or if there were no material gain available for other resonant modes, the well mode should show a clear threshold behavior. The second order mode, in the barriers, can reach a threshold condition at around 10 mA. The gain at the barrier mode is a result of the quasi-Fermi levels separation that leads to barrier pumping. Under this condition, the injected carriers into the active region are shared between the well and the barrier. It is uncertain whether the emission from the wells is lasing behavior or saturated amplified spontaneous emission.

Figure 4(c) shows the carrier density versus injected current for the well and barrier mode (solid and dashed lines, respectively). As expected for a typical laser behavior, the curves show carrier clamping for the well at the injected threshold current. Although there is a clear clamp for the carriers into the well mode, the carrier density continues rising linearly in the barrier until reaching the threshold carrier density for the barrier mode. Based on Figs. 4(c)

and 4(a), we can conclude that the carrier clamping in the wells that saturates the well mode output power indicates a carrier leakage into the barriers. Figures 4(a) and 4(c) show that the transition from spontaneous to stimulated emission (lasing threshold) becomes smoother as β increases; this is an expected result [34]. The oscillations in the QW carrier density near this transition point are due to capture and escape carrier dynamics coupled to the recombination dynamics.

If it is possible to have a material with higher gain or a cavity with lower losses (reducing the threshold gain), all the curves for the well mode would be displaced to the left in Fig. 4(a), and lasing would occur with a reduced threshold current. In the scenario with the opposite condition, if one employs a design with lower gain or a cavity with higher losses, all the curves for the well mode would be displaced to the right, with increased threshold current. This implies that the nanolasers under consideration, employing MQW gain medium, would hardly work as a laser. It should be clear that besides the inherent problem of the quasi-Fermi levels displacement until the barrier energy level, a small modification of the cavity design can drastically change the performance of the nanolaser. If the mode behavior of the first order mode is deviated from its optimal values, complete inhibition of lasing may possibly occur.

Indeed, even without the resonant mode with wavelength within the barrier bandgap, the QW mode would be saturated due to the leakage of carriers to the barriers and its spontaneous emission. A possible solution for the problem may be to change the depth of the wells and/or use other alloys, such as InGaAlAs that provides different band offsets, to avoid carrier population in the barriers. However, increasing the depth of the wells would create a second quantized level at the conduction band that also will compete for carriers. Also, it may create problems for the equalized carrier distribution amongst the wells. Therefore, the QW design for nanolasers may be extremely complex.

The same simulations were performed for the case of bulk gain medium, and the results are shown in Fig. 4(b). In this case, we have used the typical rate equations (without the reservoir model) considering a multimode solution for photons. The β -factor in this case is no higher than 0.5 for each mode because now the spontaneous emission, and consequently the stimulated emission, arises from the same material. Without this assumption the β -factor would be unphysical higher than 1. With identical β values for both modes, the spontaneous emission is equally shared between the two confined optical modes; however, the spectral density of the spontaneous emission is much higher for the first order mode and there is no available material gain for the second order mode. Consequently, the first order mode can reach the threshold around 5 mA, while there is no emission from the second order mode. The carrier density versus current injection is also shown in Fig. 4(d), where we can see a smoother clamping at threshold for the highest β .

The threshold current simulated for the bulk device is high, 5 mA, while experimental results with electrically pumped semiconductor nanolaser have reached threshold currents of only 1 mA [20]. We believe this high value is due to the surface carrier recombination that is proportional to the area/volume ratio of the active region. In our case, parts of the top and bottom surface are exposed due to the pedestal, increasing the area for surface recombination, consequently increasing the threshold current [35]. In fact, our device has a reduced volume if compared with the recorded threshold current nanolaser, which increase even more the area/volume ratio [20]. Besides that, our gain values may be slightly underestimated due to the choice of the intraband scattering time value. This does not affect our conclusions in any form.

The model applied to account for carrier leakage to the barriers in MQW nanolasers can be extended to any laser cavity with two or more confined modes. The modal properties play an important role to determine the threshold gain and for each new mode an extra photon rate equation must be added into the system of coupled equations. Independently of the number of confined modes, the modes with resonant wavelength nearest to the maximum gain will be

favorable to reach the threshold condition. Since the threshold gain for these nanolasers are very high due to the small quality factors, the leakage of carriers to the barriers will always play an important role. It is hard to predict if a higher order mode will be more propitious to lasing or not, independently of the gain media, but a cavity mode engineering can be done to increase the difference between the threshold gain of the desired mode with all the other confined modes threshold gain.

These results indicate that bulk active medium is more suitable for this class of nanolasers because it inhibits carrier losses to barrier levels that only feed higher order modes.

6. Comments on the reservoir model

To illustrate the idea of considering an interchange of carriers we use Fig. 5 that shows a simple reservoir schematic that can be useful to illustrate the role of the barrier in saturating the quantum well emission. In all figures the left reservoir is the QW and the right reservoir is the barrier. Both reservoirs are connected and can be filled with carriers (in blue) until the pump-dependent Fermi level ($\Delta\mu$, shown as a green dashed line) is reached. In Fig. 5(a), the QW starts to be filled before the barrier does, until the Fermi level $\Delta\mu_1$ is reached, since the QW has a narrower band gap than the barrier. When the pump is increased to Fermi level $\Delta\mu_2$, above the interconnection region between the two reservoirs, the barrier also starts to be populated, as depicted in Fig. 5(b). Because of the connection, the density of carriers into the wells stops increasing while there are empty states for the carriers in the barrier, as shown in Fig. 5(c). Once both reservoirs are filled to the interconnection level, they start increase together until they reach the Fermi level $\Delta\mu_3$, as shown in Fig. 5(d). The limit for filling the reservoir is the threshold condition and carrier clamping with consequent material gain clamping. The threshold condition in the figures is represented by red and blue dashed lines, for the well and for the barrier, respectively. This model is suitable to describe semiconductor nanolasers, where the lasing threshold gain is so high that this interconnection region is reached and the barrier is populated. It does not matter whether the barrier material is in the absorbing or amplifying regime, since it is sharing carriers with the well. This is the regime we have been described in this manuscript.

For larger lasers, the threshold gain (dashed red line) is expected to be much lower and will lie below the interconnection region of our model, as shown in Fig. 5(e), enabling lasing before the barrier starts to be populated. If the reservoir interconnection is far below the threshold gain for the first mode, as depicted in Fig. 5(f), only spontaneous emission will occur. Obviously, there are other effects that are not taken into account in this simple schematic. For example, the carriers are injected into the wells through the barriers; as a result, we expect a small increase in the barrier carrier density with pumping before the Fermi level reaches the interconnection region between the reservoirs.

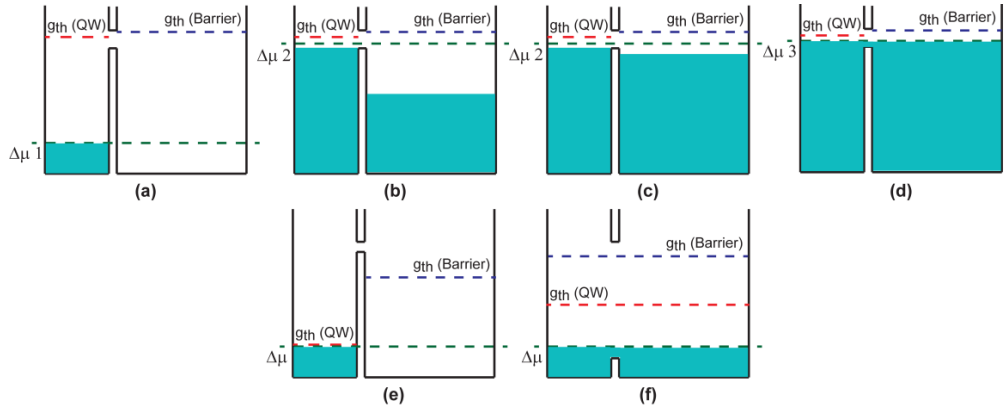


Fig. 5. Reservoir schematics to illustrate the interchange of carriers between the well and barrier. The red and blue dashed lines represents the threshold gain for the well and the barrier mode, respectively, while the green dashed line represents the pumping level $\Delta\mu$ that increases from (a) to (d). The lower figures show a reservoir where the threshold gain for the first mode is (e) lower and (f) much higher than the reservoir interconnection.

It is hard to predict the cavity dimensions where the carrier leakage starts to be detrimental for the performance of a nanolaser. It is well known that for larger MQW conventional lasers the threshold current starts to increase for cavities tens of μm 's long [28]. But such studies have never been done in the case of nanolasers, so the authors suggest to include the multi-carrier equations into the analysis of metallo-dielectric semiconductor nanolaser performance.

7. Conclusion

We discussed the advantages and disadvantages of using InGaAsP MQW as the active medium in comparison with InGaAs bulk material towards obtaining a high performance electrically pumped semiconductor nanolaser operating at room temperature. In the case of the MQW structure, we demonstrated that the level of current injection required to reach the threshold carrier density in the wells creates a highly degenerate condition where the quasi-Fermi levels displacement for electrons and holes allow the barriers to be populated. In this situation there is a clear competition for carriers between the barriers and the wells. Such competition saturates the emission from the QW mode while increasing the emission into the barrier mode. This saturation occurs independently of whether the emission from the well is stimulated or only spontaneous.

One may suggest an engineering of the multiple quantum wells to provide enough gain with a reduced carrier leakage to the barriers. The most obvious solution would be to increase the barrier height. In this case, there will be more quantized levels, which will provide transitions with shorter wavelengths and that could start to be populated before the threshold condition again saturating the emission around the desired wavelength. To avoid the second and higher quantized levels is necessary to reduce the wells thickness, but in consequence the confinement factor will also be reduced, increasing the modal threshold gain. So, the next step would be to increase the number of wells. Increasing the number of wells has the implication of creating a non uniform injection of carriers into the wells. It can also increase the volume of the active region leading to an increase of the entire laser volume. Another reasonable solution is to use strained quantum wells and barriers to increase the material gain and control the quantized levels energies. However, the defects at the interface of the strained growth material can increase the surface recombination due to possible imperfections created after the selective etching step to create the nanopillars. Besides the choice of using strained materials or performing further quantum well engineering, the design of the nanolaser becomes more complex. Since there are several implications in the design of

nanolasers with MQW gain media, the authors agree that much more work should be done to conclude if it is possible or not to have a room temperature electrically pumped metallo-dielectric semiconductor nanolaser resonators with MQW gain media, but by now the evidences shown MQW are not the best suitable material to reach this objective.

In the case of bulk structure, we have shown the fundamental mode reaches the threshold condition long before the competition for carriers with the second mode starts. The cost of using a bulk gain media to avoid the second order mode is a higher threshold current in comparison with the MQW device. This threshold current can be reduced if the bulk ternary alloy is substituted by a bulk quaternary alloy whose available material gain is within the optimized threshold gain for a specific cavity.

These results show that while quantum well structures allow large semiconductor lasers to have very low threshold current, they can inhibit lasing action in high gain demanding nanolasers due to a competition between wells and the barriers for injected carriers. Although the optical gain for bulk material is smaller and the transparency carrier density is larger than for MQW structures, the high threshold gain and the barrier pumping problem makes bulk gain media more suitable for obtaining room temperature electrically pumped metallo-dielectric semiconductor nanolaser resonators.

Acknowledgments

The authors would like to thanks Janelle Shane and Luís Alberto Mijam Barea for helpful discussions. This work was supported by the Brazilian financial agencies: CNPq, CAPES, Center for Optics and Photonics (CePOF) under grant # 05/51689-2 and National Institute for Science and Technology (FOTONICOM) under grant #08 /57857-2, São Paulo Research Foundation (FAPESP). This work was also supported by the Defense Advanced Research Projects Agency (DARPA), the National Science Foundation (NSF), NSF through Center for Integrated Access Networks (CIAN) NSF ERC under grant #EEC-0812072, the Cymer Corporation, and the U.S. Army Research Office.